1986A&AS...65..465P

ASTRONOMY & ASTROPHYSICS
SUPPLEMENT SERIES

Astron. Astrophys. Suppl. Ser. **65,** 465-484 (1986)

CO $J = 2 - 1$ observations of three southern star formation regions (*)

J. P. Phillips (1), C. P. de Vries (2) and T. de Graauw (3)

(1) Physics Department, Queen Mary College, Mile End Road, London E1 4NS, U.K.
(2) Sterrewacht, P.O. Box 9513, 2300, RA Leiden, The Netherlands
(3) Laboratory for Space Research, Postbus 800, 9700 AV Groningen, The Netherlands

Received April 9, accepted December 2, 1985

Summary. — We present CO $J = 2 - 1$ mapping and spectroscopy for three southern star-formation regions. In one of these, NGC 6334, we find broadly similar line strengths and profiles to those at $J = 1 - 0$, and use both these, ^{13}CO $J = 1 - 0$ measures, and various assumptions concerning the dynamical state of the gas to place constraints upon masses, densities, and velocity gradients in the primary star formation centres. NGC 6193 appears to contain a compact CO cloud with rather interesting dynamical properties. Given the relative youth of this cluster, it is possible that we are witnessing compression and dissipation of placental material by protostellar winds. The level of disruption however appears to be quite modest, with line cores having typical widths < 3 km.s^{-1}. Finally, the moderately bright rim structure IC 4628 is shown to define the edges of a warm and extensive CO cloud, with gas kinetic temperatures exceeding $T_k \sim 30$ K, and overall size > 45 arcmin. The main heating for this cloud probably derives from several strong embedded FIR sources, although contributions from a scattering of lower luminosity stars may also be important. The integrated line strength is found to take a maximum close to the associated cluster Tr 24.

Key words : CO $J = 2 - 1$ — mapping — star-formation regions.

1. Introduction.

The inception of large ground-based observing facilities in the southern hemisphere has led to a renaissance in observations of southern star-formation regions. Until recently, however, there was a relative paucity of observations at millimetre and submillimetre wavelengths, and the earliest CO measurements (of the Magellanic clouds at $J = 1 - 0$) were acquired as recently as 1975 (Huggins *et al.*, 1975). This anomaly is now rapidly being corrected, however, and programmes involving large scale surveys (cf. Robinson *et al.*, 1983 ; Israel *et al.*, 1984) and more detailed mapping of individual complexes (cf. various contributions in Burton and Israel, 1983) have been instituted by several groups. The present work concerns three rather differing types of region in the declination range $-50° <$ and $< -35°$. The most northerly of these sources, NGC 6334, is an extensive complex of five or so star formation centres within a larger enveloping cloud. This complex is accessible from northern facilities at fairly large air masses, and has been mapped by Dickel *et al.* (1977) in the $J = 1 - 0$ transition for CO. The other complexes to be considered here however have not (to our knowledge) been the subject of detailed examination at these frequencies. One, IC 4628, is a bright rim structure similar to the classical nebulae identified by Pottasch (1956), and investigated at millimetre wavelengths by Wootten *et al.* (1983). The remaining source is centred upon the cluster NGC 6193, a compact and relatively young stellar system which is immersed in nebulosity, and lies close to an ionisation ridge. For all of these regions there is a variety of evidence for extensive and continuing star forming activity.

The present CO $J = 2 - 1$ results were acquired with the ESTEC/Utrecht heterodyne millimetre wave receiver mounted on the 3.6 metre ESO telescope at La Silla. The half-power beamwidth was measured to be 1.9 arcmin, beam efficiency was 0.60, the DSB noise temperature was of order 2000 K, and the measured antenna temperature of Ori A was 64 K. A more detailed description of instrumental parameters, observing and calibration procedures is provided in Brand *et al.* (1984), and the receiver and backend are described by Lidholm and de Graauw (1979). Offset positions were generally 2 degrees above or below the sources being measured, at locations where the CO $(J = 2 - 1)$ emission was found to be negligible, and the velocity resolution was in all cases 0.33 km.s^{-1}. The present results have not been

(*) Based in part on observations collected at the European Southern Observatory.

Send offprint requests to : J. P. Phillips.

© European Southern Observatory • Provided by the NASA Astrophysics Data System

1986A&AS...65..465P

smoothed, although a linear baseline has been subtracted from most spectra.

In the following, we consider the three star-formation centres separately.

2. NGC 6334.

The NGC 6334 complex is located at a distance of 1.74 kpc (Neckel, 1978), and represents an area of extensive and complex nebulosity, maser activity, and HII regions on a variety of size scales. The cloud was one of the earliest to be mapped at far-infrared wavelengths (Emerson *et al.*, 1973), and has been the subject of several similar and more refined investigations over subsequent years (cf. McBreen *et al.*, 1979 ; Rodriguez *et al.*, 1978). It is apparent from this work that the primary nebulosities identify locations of multiple near- and far-infrared sources (Harvey and Gatley, 1983 ; Becklin and Neugbauer, 1974), and represent peaks in CO (Dickel, 1977), far-infrared (Rodriguez *et al.*, 1978 ; McBreen *et al.*, 1979 ; Emerson *et al.*, 1973) and millimetre continuum emission (Cheung *et al.*, 1978). The area, in short, contains a considerable range and variety of star-forming activity.

We have extensively sampled this region in CO $J = 2 - 1$, and in certain cases measured the same positions to those by Dickel *et al.* (1977). The beam locations are illustrated on an SERC Southern Survey plate of the region in figure 1, where we have also identified IRAS point source positions. Individual spectra for the CO peak positions (and intermediate points) are illustrated in figure 7a, and the comparative $J = 1 - 0$ results from Dickel *et al.* (1977) are provided in figure 7b. A numerical summary of figure 7a is also provided in table I (where labels A → D correspond to the terminology of Dickel *et al.*, 1977). Also provided in table I are comparative estimates of T_A^* $(J = 1 \rightarrow 0)$ for ^{13}CO and CO, taken from the published spectra of Dickel *et al.* These are generally larger than the values tabulated by Dickel *et al.*, who used Gaussian fits to parametrize what are often strongly non-Gaussian profiles. The difference between these two sets of estimates is often appreciable, although the discrepancies do not appear to exceed ~ 10 % in the mean. Note, also, that whilst the velocity of peak emission shifts around quite substantially, it remains closely similar for all of the transitions. A direct comparison of peak temperatures at the same locations (see later) is therefore entirely reasonable.

Spatial-velocity maps for the four primary traverses in figure 1 are provided in figures 2-5. The first of these maps, in figure 2, passes through the northernmost CO peak (although there is evidence for a density and 1 mm continuum maximum approximately 2 arcmin further north of this position (cf. Cheung *et al.*, 1978 ; Rodriguez *et al.*, 1982 (NH_3) ; Turner and Thaddeus, 1977 (NH_2^+) ; Dickel *et al.*, 1977 (H_2CO))). The peak is associated with H_2O (Meeks *et al.*, 1969 ; Knowles *et al.*, 1969 ; Sullivan, 1973) and OH (Weaver *et al.*, 1969) masers, and contains at least four infrared components with a combined luminosity ~ $1.5 \times 10^5 L_\odot$ (Harvey and Gatley, 1983). The dominant component (IRS 1 in the parlance of Harvey and Gatley, 1983) is associated with low level of radio emission, and appears to represent a likely protostellar candidate. The 20 μm and 30 μm infrared maps of this region are similar to the radio continuum map of Rodriguez *et al.* (1982), which is in turn reminiscent of the classical blister structures investigated by Israel (1978) and others.

The present results confirm the sense of the $J = 1 - 0$ measures by Dickel *et al.* (1977), although both at this and other positions the $J = 2 \leftarrow 1$ line strength is some ~ 20 % weaker. Much of this may result from beam dilution effects, which we estimate would typically contribute a ~ 10 % weakening of the $J = 2 - 1$ lines relative to $J = 1 - 0$. Systematic calibration differences between the two sets of observations may presumably also be similar, and it is clear that much of the disparity in line strengths may be accounted for through these external factors alone. In the following analysis, we will assume a mean relative correction of ~ 1.1 to allow for these effects — uncertainties of ~ 10 % or so do not greatly effect our conclusions. The lineshapes vouchsafe very closely similar kinematic structures for the two CO transitions, and this comparability is faithfully replicated throughout the NGC 6334 cloud. Nevertheless, the linewidth $\Delta V\,(2-1)$ is broader than $\Delta V\,(1-0)$ by ~ 13 % ; similar again to the mean ratio throughout the complex (~ 23 %). We will discuss the possible reasons for the trend later this section.

To the north of the emission peak (and traversing the density maximum noted earlier) there is a marked reduction in line velocity width, and a gradual reduction in line intensity towards the putative cloud edge. Much of this northernmost extension is presumably heated by source A, and there is little evidence to support more extensive heating from embedded secondary star-formation centres. The southern limit of our map occurs uncomfortably close to the peak emission core, although it is nevertheless clear that the emission fall-off is significantly steeper than to the north. Dickel *et al.* (1977) suggest the presence of an extensive, although low-level $J = 1 - 0$ wing extending ~ 5 arcmin below our map.

Two further features should finally be registered : the evidence for a weak intensity dip at ≈ -5 km.s^{-1}, apparently present in all of our spectra. This is a barely detected feature, although its persistence suggests the presence of a weak and wide-ranging self-absorption core. The second important characteristic is that, as in most of the cases measured here, the mass-condensation resides at a similar V_{lsr} to that of the (cooler) ambient material.

This is *not* however the case in our next map, reproduced in figure 3, and corresponding to source B. As in all of the CO maxima, this peak corresponds to an area of strong optical emission (see Fig. 1). It is also associated with a 70 μm emission peak in the map of McBreen *et al.* (1979), a 40-350 μm peak in the mapping of Rodriguez *et al.* (1978), and a 1 mm continuum maximum (Cheung *et al.*, 1978). The radio source is significantly extended and non-spherical (Rodriguez

© European Southern Observatory • Provided by the NASA Astrophysics Data System

1986A&AS...65..465P

et al., 1982), and Harvey and Gatley (1983) interpret their IR map in terms of an evolved nozzle source. The condensation in this case is clearly moving at a significant relative velocity compared with adjacent emission zones, although the extension of the emission peak towards the north implies local heating of this gas by source B. There is, in short, a *prima facie* case for supposing that source B is moving *through* the ambient material, rather than representing a feature on the near-side of a collapsing cloud (Dickel *et al.*, 1977). The distinct velocity shift corresponding to this condensation is also seen in figure 7a.

Finally, the maps in figures 4 and 5 represent more limited traverses through condensations C and D. Condensation C (Fig. 4) has a FIR luminosity $\sim 2 \times 10^5\, L_\odot$. Harvey and Gatley (1983) find a total of six sources in this zone, three showing evidence for self absorption at 10 μm (IRS 2, 3 and 4), and one (IRS 1) which appears to represent a protostar. Various other local indictors, including an H_2O maser source, a Herbig-Haro object (Gyulbudaghian *et al.*, 1978), strong 70 μm and 40-350 μm peaks, and maxima in NH_2^+, HCN, HCO^+, and CS emission (Turner and Thaddeus, 1977 ; Gardner and Whiteoak, 1978) imply the presence of vigorous star formation and dense mass concentrations. A radio source associated with this region (Rodriguez *et al.*, 1982) is centred upon the source IRS 2 of Harvey and Gatley, and appears as a compact ($\sim 10''$) shell structure. Source D by way of contrast (Fig. 5) probably corresponds to a single point source embedded in a 20-30 μm east-west emission ridge. There is no associated compact radio source (Rodriguez *et al.*, 1982) or indeed *any* appreciable local radio emission, fuelling suggestions that this too is a protostar.

This whole complex has been represented in terms of mass condensations within a collapsing cloud (Dickel *et al.*, 1977). Feature B, for instance, is proposed to reside in the near half of this region, whilst the neighbouring condensation C is located midway through the enveloping cloud. The outermost pair of condensations is presumed to be placed towards the rear of the cloud (as viewed from Earth), in conformity with their more positive radial velocities. The typical velocity difference $V\left(^{12}\mathrm{CO}\right) - V\left(^{13}\mathrm{CO}\right) \simeq 0.75$ km.s^{-1} for the *condensations* however suggests that these, at least, are close to dynamical equilibrium, or perhaps even expanding somewhat. There is precious little evidence to favour collapse at the star formation centres themselves.

This is hardly surprising, since well-rehearsed arguments concerning the star-formation rate would appear to preclude detection of widespread collapse (cf. Field, 1978 ; Zuckerman and Palmer, 1974). Indeed, so restrictive are these arguments that we can expect to see no more than 1 in ~ 70 large clouds in the process of rapid contraction (where we have used the most recent information on star forming efficiency, etc.). It is improbable on these grounds alone, therefore, that the NGC 6334 complex can be globally unstable, and there are also various other (weaker) arguments which support this contention.

A condensation deeply embedded in the larger enveloping cloud, for instance, might be expected to be appreciably extinguished by $A_v \sim$ several tens of magnitudes (see later — this is also expected with the Dickel *et al.* cloud parameters). However, bright optical emission is seen at each of the CO peaks. This is particularly the case with source A, which according to Dickel *et al.* (1977) should be the most extinguished. Similarly, and as noted earlier, source B appears to be heating local gas, which is in turn moving at an appreciably more negative velocity. It is not clear how this could be reconciled with a simple collapse model, short of arguing for a coincident foreground source a little to the north of B.

In short, therefore, whilst the model described by Dickel *et al.* (1977) was carefully argued, and remains an interesting option, it is clear that other structures might also be profitably considered. In the case of condensation B, for instance, an embedded outflow source may contribute to compression and acceleration of the ambient material, resulting in the rather sharp variations in line kinematics for this region. Alternatively, small velocity differences may simply reflect the consequences of virial equilibrium ; the cloud and condensations forming a single, self-gravitating system. There is no reason (on this scenario) for the star formation centres to be located in any particular zone.

The various presently available CO line intensities do not enable unique solutions to be determined for $n\left(\mathrm{H_2}\right)$ or $X(\mathrm{CO})/\mathrm{d}v/\mathrm{d}z$ (where $X(\mathrm{CO})$ is the abundance of CO relative to H_2, and $\mathrm{d}v/\mathrm{d}z$ is the line of sight velocity gradient), although the range of possibilities can be greatly restricted. This is illustrated in figure 8, where the areas of solution for an LVG model are given, and mean values of

$$Q = T_A^*(J = 2-1)\,/\,T_\mathrm{A}^*(J = 1-0)$$

and $T_\mathrm{A}^*\left(^{13}\mathrm{CO}, J = 1-0\right)$ for the data set in figure 7 are outlined. In this case, it is apparent that the typical cloud region as defined above would have $n\left(\mathrm{H_2}\right) > 4 \times 10^3$ cm^{-3} and $X/\mathrm{d}v/\mathrm{d}z < 5.0 \times 10^{-5}$ km^{-1} s.pc. A corresponding turbulent analysis would also be expected to lead to very similar results given that $\mathrm{d}v/\mathrm{d}z \equiv \Delta V_\mathrm{TURB}/2R$, where $2R$ is the depth of region under consideration, and ΔV_TURB the relevant range of turbulent velocities (determined from optically thin line profiles, cf. White, 1977). To obtain more restrictive solutions however requires further constraints.

For the present case, we shall assume that the velocity range through a source with radius R is $\Delta V \simeq (4\,GM/R)^{1/2}$, where M is the corresponding mass. From this it follows that

$$\left\langle \frac{\mathrm{d}V}{\mathrm{d}Z} \right\rangle \sim \frac{\Delta V}{2R} \simeq 3.0 \times 10^{-2} \left\langle n\left(\mathrm{H_2}\right)\right\rangle^{1/2} \mathrm{km.s^{-1}.pc^{-1}} \quad (1)$$

and

$$\left\langle \frac{X\langle \mathrm{CO}\rangle}{\mathrm{d}v/\mathrm{d}z} \right\rangle \approx \frac{3.36 \times 10^{-3}}{\left\langle n\left(\mathrm{H_2}\right)\right\rangle^{1/2}} \mathrm{km^{-1}.s.pc} \quad (2)$$

© European Southern Observatory • Provided by the NASA Astrophysics Data System

1986A&AS...65..465P

where we have taken $X(CO) \simeq 10^{-4}$ (cf. Goldsmith *et al.*, 1980), and $\langle n(H_2) \rangle$ is the mean H_2 number density within radius R — a value which should also be reasonably representative of the mean CO excitation density. Expression (1), although straightforward in both application and derivation, has nevertheless a rather wide applicability. It is relevant for instance where there is rotational equilibrium, and also applies (to within small factors) where clouds are in turbulent or thermal pressure equilibrium, or a state of free-fall collapse. The expression cannot however be applied where strong non-equilibrium interactions are occurring, due to say stellar winds, expanding HII regions, and so forth — a situation which may be particularly relevant for condensation B. If the various hot-spots in NGC 6334 can therefore be characterised as spheroidal, centrally heated non-disrupted clouds, then an analysis based upon the above constraints should be reasonably informative.

The variation of this relation in the $X(CO)/dv/dz$, $n(H_2)$ plane is illustrated in figure 8. We have also used these constraints to isolate specific solutions for the various cloud regions in figure 7a. The results of this analysis are presented in table I, where in addition to dv/dz and $n(H_2)$ we give the line of sight depth Z, and (based upon this) the overall mass $M/M_\odot$, and extinction A_v $(= 10^{-21} N(H_2))$. Local gas kinetic temperature was in all cases assessed from the strength of the $J = 1 \rightarrow 0$ lines (i.e. populations in the relevant CO rotational levels are determined through collisions with H_2).

The primary constraint upon our solutions is provided by the ^{13}CO data of Dickel *et al.*, although the present analysis (and parameters such as distance) are different. The results also confirm (at least in qualitative form) the physical parameters deduced by Dickel *et al.* The velocity gradient dv/dz (or $\Delta V_{TURB}/2R$) for instance is required to be steep at the condensations. Immediately outside the condensations, however, dv/dz settles down to a value slightly in excess of 1 km.s^{-1}.pc^{-1}. This value is, of course, similar to the large scale gradients observed in other clouds, and remains remarkably consistent over the measured region. Extinction through the enveloping cloud appears to be of order 20-30 magnitudes in the visible, although this peaks up at the condensations, and is perhaps as high as 280 mags at source A. The deduced cloud masses are particularly susceptible to the errors and uncertainties of this analysis, however, and should perhaps be taken as reliable at the order of magnitude level only. In this case we have adopted $M \simeq 2.6 \times 10^{-2} (Z/pc)^3 n(H_2) M_\odot$. The estimate of M for source A however is closely similar to that found by Dickel *et al.*, and the other values also appear broadly plausible. It would seem from this, therefore, that the condensations contain an appreciable proportion of the total cloud mass, and have individual masses of order $> 10^3 M_\odot$.

We might at this point emphasize, however, that whilst the assumption of spherical symmetry for the condensations is analytically convenient, it can hardly accord with reality ; the structure of source A for instance implies a blister-like formation, which would almost certainly result in a non-symmetric enveloping neutral zone. More serious, however, is the fact that optical emission at locations A through D is not reconciliable with the high extinctions determined in table I, unless the mass structures are again appreciably non-symmetric. Whilst the estimates of mass determined above are therefore still broadly plausible, it is clearly important to improve on this analysis when more (and better resolution) observations become available.

Finally, we note that application of the modelling of Phillips *et al.* (1981) to the $J = 2 - 1$ and $J - 1$ CO results suggests an optical depth $\tau_{1-0}(CO) \sim 6$. This analysis assumes variations in line width to result from saturation effects, and a comparison of ^{13}CO and ^{12}CO line strengths suggests that the actual value of $\tau_{1-0}(CO) \simeq 18$ is not inconsistent with this hypothesis (where we have adopted a ratio $^{12}C/^{13}C \sim 67$; Penzias, 1979). However, ^{13}CO linewidths appear not to be greatly different from those measured for the main isotope, and this would *not* be predicted by the line saturation model. It is likely therefore that variations in $\Delta V(^{12}CO, J - J - 1)$ are due primarily to differences in beamsize.

3. NGC 6193.

NGC 6193 is a rather compact cluster dominated by the O stars HD 150136 and HD 150135, and represents a core for the more widespread ARA OB1 association. Evidence for recent star formation is fairly widespread, and the age of the central cluster itself can barely exceed $\sim 10^6$ years. In consequence, many of the fainter cluster members appear still to be contracting onto the main sequence (Herbst and Havlen, 1977). The IRAS survey reveals a sparse litter of (predominantly) near- and mid-infrared sources scattered uniformly about (and within) the cluster (IRAS Point Source Catalogue, JPL, 1980). Many of these presumably represent stars embedded in placental material, and the northernmost pair are of particular interest in this regard. Both appear to be associated with visual counterparts, and are located on the edge of a clearly defined wind-swept globule. Whether they represent a chance encounter of globule and stars or, more likely, are the products of (shock induced ?) star formation is not entirely clear. Their simularity to the (protostellar) sources identified by Reipurth (1983) however is striking, with the driving wind in this case arising from the vicinity of NGC 6193. Indeed, as we will see, a CO cloud near the cluster may also be in the process of disruption, perhaps by the self-same outflow. Further observations of these sources would clearly be of considerable interest.

The brightest source in the region however is RCW108, located some 13 arcmin west of the cluster, and closely adjoining an ionisation front which runs the length of our photograph (Fig. 9). This very well studied source has been mapped in the infrared by Frogel and Persson (1974), and observed in CO by Gillespie *et al.*

© European Southern Observatory • Provided by the NASA Astrophysics Data System

1986A&AS...65..465P

(1977), and appears to represent a protostar with luminosity L ($< 100\ \mu m$) $\sim 3.6 \times 10^5\ L_\odot$ (Fig. 6). Several of the other strong FIR sources in figure 9 probably also represent protostars, although it is interesting to note that the claimed protostellar source of Herbst and Havlen (1977) (near the central O stars) does not show in the IRAS point source catalogue. Similarly, none of the IR sources of Tapia (1981) (which appear to be located in and about the CO cloud) can clearly be correlated with IRAS detections.

We have mapped an area of the source about the cluster centre in CO ($J = 2 - 1$), and find evidence for a relatively compact emission source centred south-east of the O stars, and close to star 147 of Herbst and Havlen (1977), and the coincident IRS 2 of Tapia (1981). Herbst and Havlen identify this as a G5 foreground star, and the implied V-K of $\simeq 1.8 \pm 0.2$ mags is consistent with this spectral type. If the star were a cluster member, however, then it would have to be both luminous and strongly pre-main-sequence ; although the absence of an associated IRAS source mitigates against this hypothesis. Spatial-velocity slices through the cloud are illustrated in figures 10-12, and correspond to the various axes drawn in figure 9. Declination strips to the west of centre indicate a relatively narrow and compact profile, and it appears that the cloud at this location is kinematically inactive (Fig. 10). A slice along the R.A. axis however (Fig. 11) shows a rather interesting trend towards the cloud centre. The bulk of the emission is displaced in velocity by $\sim +1\ km.s^{-1}$, whilst a weak velocity wing of width $\Delta V \simeq 5\ km.s^{-1}$ is seen to extend to more negative velocities. This characteristic is further illustrated in figure 12, corresponding to an orthogonal N-S strip through the centre.

The model for this region that we presently favour envisages the compression of local material by a stellar wind, which in turn emanates from a location close to the (projected) G5 star. A schematic diagram of this scenario is provided in figure 13, wherein a very much more massive rear cloud is accelerated to velocities $\sim +1\ km.s^{-1}$ (relative to the unshocked gas). The foreground shell responsible for the wing emission is presumed to be very much less massive, and more disrupted, in consequence of which displacement velocities are greater, and antennae temperatures lower.

The nature of the molecular cloud and its relation to NGC 6193 are uncertain, although it is clearly tempting to regard it in terms of placental material which has yet to fully evacuate the cluster. If this is true, however, then the cloud is remarkably inactive from the kinematic point of view, with line widths typically $< 3\ km.s^{-1}$.

The alternative situation whereby the cloud completely envelopes the (optical) cluster would require a low CO excitation density, or alternatively a large value for the ratio $N(H_2)/A_v$. From the optical/near-red photometry of Herbst and Havlen (1977), for instance, and assuming the central cluster stars to be uniformly distributed throughout an homogeneous HI cloud, we determine a maximum central extinction $A_v \simeq 2.4$ mags (allowing for $A_v \sim 0.66$ mags of foreground interstellar extinction). Under these circumstances, the central extinction takes a value $A_v \simeq 1.5\,\bar{A}_v$, where $\bar{A}_v$ is the mean local extinction for the cluster stars. Given a distance 1320 pc (Herbst and Havlen, 1977) and a « normal » ratio $A_v/N(H_2) \sim 10^{-21}$ mags, we then determine a typical H_2 density $\langle n(H_2) \rangle \sim 500\ cm^{-3}$. This is very much less than usually observed in clouds with strong CO ($J = 2 - 1$) emission, and would imply appreciably non-thermalised lines.

Note, finally, that there is no evidence for FIR (or indeed NIR) point source emission from anywhere within the CO cloud. Any outflow source cannot therefore be particularly luminous, and/or located near appreciable masses of dust. Similarly, whilst it is probable that many (low mass) stars in this region represent pre-main-sequence objects, continuing star-forming activity appears to be weak to non-existent.

4. IC 4628.

IC 4628 represents an extended region of moderately intense nebular emission, forming for much of its length a fairly well defined bright rim (Fig. 14). Within this region is the small cluster Tr 24 dominated by the O6 star HD 152723, which is presumably also responsible for much of the local ionisation and Hα emission (cf. Gum, 1955). More widespread (~ 4 degrees) Hα emission covers this entire region, and appears to be excited by the SCO B1 association and NGC 6231, some 1.5 degrees to the southwest. The exciting source for the bright rim however is rather less obvious, although the brightest FIR source in the region (B in Fig. 14) lies just a little to the north. Perhaps the relevant star(s) remain hidden behind the rim, and there are certainly several (moderately strong) NIR and FIR sources scattered throughout this zone (A, F, and G). Alternatively, Gum (1955) has pointed to several faint O-stars within the nebulosities which may also contribute to local excitation.

In either case, the star or stars must have a (combined) excitation parameter > 34, based on the H109α survey of Wilson *et al.* (1970), and this would correspond to excitation by a single BO-O.5I or 09V star (Panagia, 1973).

Tapia (1981) has published near-infrared photometry for various IR sources in Tr 24, indicating stellar continuum reddening by $A_v \sim 13$ mags. Danks (1975) has also found a star close to the bright rim through K-band scanning, and identified it as a heavily reddened supergiant. The position of this source corresponds closely to that of a near-infrared IRAS source (marked A in Fig. 14), and the combined continua are illustrated in figure 6. If, improbably, the IRAS source does not correspond to the Danks' object, then we must suppose it to be fainter than the limits of the Danks' survey at K — which would make it even more interesting.

It would appear, from these combined results, that the continuum of this object peaks close to $\lambda \sim 12\ \mu m$. This is unlikely to result solely from reddening of a normal stellar continuum, since a) the reddening would be

© European Southern Observatory • Provided by the NASA Astrophysics Data System

1986A&AS...65..465P

required to be of order $A_v \sim 10^2$ mags, and the source inordinately bright, and b) there is no associated FIR excess. More plausibly, one might suppose the star to have a strong mid-infrared excess (due to silicate band emission ?), or that it is variable. For either circumstance, however, it is clear that further analysis should predicate upon more accurate and contemporaneous NIR data.

Our CO beam positions are indicated in figure 14, and the corresponding spatial-velocity map is illustrated in figure 15. As for other bright rim sources (cf. Wootten, 1983), a warm CO cloud is found within the convex rim of IC 4628. This appears to extend over a length of ~ 24 arcmin, although there is also evidence for weaker emission to the north of the rim. The relatively high temperatures of ~ 30 K approached in this traverse indicates considerable cloud heating, dominated in all probability by the IRAS sources B and C (to the north), and D and E (to the east). In addition to these, NIR sources appear to be scattered throughout the cloud region, testifying to more widespread heating by lower luminosity stars, and the possibility of more extensive star-forming activity away from the areas of nebulosity.

From figures 15 and 16 it is apparent that the CO velocity width declines towards the north. Antennae temperatures T_A^*, and line integrals $\int T_A^* \, dv$ also vary somewhat, with T_A^* peaking a little inside the rim, and the line integral taking a maximum towards the south, in the vicinity of cluster Tr 24. There is a possibility, therefore, that stars in Tr 24 are directly associated with an increased kinematic activity within the cloud. In particular, it may be noted that the dominant O star HD 152723 lies very close to our traverse, to the position of maximum integrated line strength, and to a (possibly related) NIR source. Rim excitation may also be associated with a direct temperature increase in the HI zone. Much of the variation of T_A^*, however, can probably be attributed to reduced collisional excitation in areas of lower density $\left(n\left(H_2\right) < 10^4 \text{ cm}^{-3}\right)$, particular towards the fringes of the cloud.

Finally, the central line velocity V_{lsr} is notable for its relative constancy over this region. Projected velocity changes amount to no more than ~ 0.5 km.s^{-1}, and for a cloud in rotational equilibrium this would imply a total mass $M \sim 234\, M_\odot$, and mean density $\langle n\left(H_2\right)\rangle \sim 4$ cm^{-3}. Clearly, neither of these derived quantities are plausible, and it is probable that either a) cloud rotation is not important for the equilibrium properties of this region — the cloud is either collapsing, or suspended by turbulent, magnetic, and/or thermal pressure terms, or b) the vector for increasing V_{lsr} lies roughly perpendicular to the present traverse. If, alternatively, we assume the line widths to reflect turbulent broadening, and the cloud to be in a state of turbulent pressure balance, then we find $\langle n\left(H_2\right)\rangle \sim 1.6 \times 10^3$ cm^{-3}, and a total extinction through the cloud of $A_v \sim 40$ mags.

Overall, therefore, the region of IC 4628 appears to be one of extensive star formation, nebulosity, and numerous FIR sources. It also contains at least one substantial CO cloud delineated partially in the present survey, and covering an area of ≈ 0.3 square degrees or greater (assuming the RA extension to be at least comparable). Whilst the cloud is warm, it appears to be kinematically only moderately active in the regions surveyed, with line widths generally less than ~ 5 km.s^{-1}.

5. Conclusions.

We have presented spatial-velocity and spatial maps of three southern star formation regions in $J = 2 - 1$ transition of CO. One of these regions, the more northernly of the three, is the fairly well observed NGC 6334, a cloud which has already been mapped by Dickel *et al.* (1977) at $J = 1 - 0$. Our $J = 2 - 1$ profiles show closely similar profiles to the $J = 1 - 0$ results where observations were taken at similar locations, and a simple kinematic model is used with ^{12}CO $(J = 1 - 0)$, ^{12}CO $(J = 2 - 1)$, and ^{13}CO $(J = 1 - 0)$ data to place constraints upon the properties of the star formation centres. Broadly speaking, it appears likely that the CO peaks correspond to mass concentrations of $\sim 10^3\, M_\odot$ or more, and velocity gradients $dv/dz \sim 2$ km.s^{-1}.pc^{-1}. Extinctions and densities in these regions appear also to be large, taking the respective (typical) values $A_v \simeq 36$ mags, and $n\left(H_2\right) \sim 3 \times 10^3$ cm^{-3}, although these fall to $A_v \sim 25$ mags and $n\left(H_2\right) \sim 1.7 \times 10$ cm^{-3} in the enveloping cloud. Source A may be exceptional however in having $A_v \sim 300$ mags and $n\left(H_2\right) \sim 6 \times 10^4$ cm^{-3}.

The second star formation region to be considered here was centred upon NGC 6193. In this case we observed a moderately strong and compact CO source close to the primary O stars SAO 227049 and SAO 227048. Given the relative youth of this cluster ($< 10^6$ years) it is conceivable that we are observing remnants of the cluster placental material. This, in turn, may be being disrupted by stellar winds from the projected vicinity of SAO 227053, a probably foreground G5 star.

The final region to be investigated was IC 4628. This bright rim nebula appears to contain a relatively warm CO cloud, approaching CO $J = 2 - 1$ antennae temperatures of ~ 30 K along a traverse through the cluster Tr 24. The lines are moderately broad, with evidence for a weak decrease towards the northern cloud rim. The primary heating source for this cloud is probably to be found in several bright embedded sources, although a scattering of NIR objects suggests a contribution from lower luminosity stars. In addition, the maximum integrated line strength is found to occur close to the cluster Tr 24, and this may reflect direct local heating by the cluster stars, a kinematic disturbance due to stellar winds, or some related input of mechanical or thermal energy.

© European Southern Observatory • Provided by the NASA Astrophysics Data System

1986A&AS...65..465P

References

BECKLIN, E. E., NEUGEBAUER, G. : 1974, *Proceedings of the Eigth ESLAB Symposium,* eds. A. F. M. Moorwood (Neuilly-sur-Seine : ESRO), p. 39.
BURTON, W. B., ISRAEL, F. P. : 1983, *Surveys of the Southern Galaxy,* eds. D. Reidel Publishing Co. (Dordrecht, Holland).
BRAND, J., VAN DE BIJ, M. D. P., DE VRIES, C. P., ISRAEL, F. P., DE GRAAUW, Th., VAN DE STADT, H., WOUTERLOOT, J. G. A., LEENE, A., HABING, H. J. : 1984, *Astron. Astrophys.* **139,** 81.
CHEUNG, L., FROGEL, J. A., GEZARI, D. Y., HAUSER, M. G. : 1978, *Astrophys. J.* **226,** L149.
DANKS, A. C. : 1975, *Publ. Astron. Soc. Pac.* **87,** 941.
DICKEL, H. R., DICKEL, J. R., WILSON, W. J. : 1977, *Astrophys. J.* **217,** 56.
EMERSON, J. P., JENNINGS, R. E., MOORWOOD, A. F. M. : 1973, *Astrophys. J.* **184,** 401.
FIELD, G. C. : 1978, *Protostars and Planets,* eds. T. Gehrels (University of Arizona Press, Tucson, Arizona).
FROGEL, J. A., PERSSON, S. E. : 1974, *Astrophys. J.* **192,** 351.
GARDNER, F. F., WHITEOAK, J. B. : 1975, *Mon. Not. R. Astron. Soc.* **183;** 711.
GILLESPIE, A. R., HUGGINS, P. J., SOLLNER, T. C. L. G., PHILLIPS, T. G., GARDNER, F. F., KNOWLES, S. H. : 1977, *Astron. Astrophys.* **60,** 221.
GOLDSMITH, P. F., LANGER, W. D., CARLSON, E. R., WILSON, R. W. : 1979, *I.A.U. Symposium* **87,** eds. B. H. Andrew (D. Reidel Publishing Co., Dordrecht, Holland).
GUM, C. S. : 1955, *Mem. R. Astron. Soc.* **67,** 155.
GYULBUDAGHIAN, A. L., GLYSHKOV, Yu. I., DENISYUK, E. K. : 1978, *Astrophys. J.* **224,** 437.
HARVEY, P. M., GATLEY, I. : 1983, *Astrophys. J.* **269,** 613.
HERBST, W., HAVLEN, R. J. : 1977, *Astron. Astrophys. Suppl. Ser.* **30,** 279.
HUGGINS, P. J., GILLESPIE, A. R., PHILLIPS, T. G., GARDNER, F., KNOWLES, S. : 1975, *Mon. Not. R. Astron. Soc.* **173,** 69 p.
ISRAEL, F. P. : 1978, *Astron. Astrophys.* **70,** 769.
ISRAEL, F. P., DE GRAAUW, T., DE VRIES, C. P., BROND, J., VAN DE STADT, H., HABING, H. J., WOUTERLOOT, J. G. A., VAN AMERONGEN, J., VAN DE BIEZEN, J., LEENE, A., NAGTEGAAL, I., SELMAN, F. : 1984, *Astron. Astrophys.* **134,** 396.
KNOWLES, S. H., MAYER, C. H., SULLIVAN, W. T., CHEUNG, A. C. : 1969, *Science* **166,** 221.
LIDHOLM, S., DE GRAAUW, Th. : 1979, *First International Conference on Infrared and Multimetre Waves and their Applications,* eds. Perkowitz, p. App. 38.
MARSALKOVA, P. : 1974, *Astrophys. Space Sci.* **27,** 3.
MCBREEN, B., FAZIO, G. G., STIER, M., WRIGHT, E. L. : 1979, *Astrophys. J.* **232,** L183.
MEEKS, M. L., CARTER, J. C., BARRETT, A. H., SCHWARTZ, P. R., WATERS, J. W., BROWN, W. E. : 1969, *Science* **165,** 180.
NECKEL, T. : 1978, *Astron. Astrophys.* **69,** 51.
PANAGIA, N. : 1973, *Astron. J.* **78,** 929.
PENZIAS, A. A. : 1979, in *I.A.U. Symposium* **87,** eds. B. H. Andrew (D. Reidel Publishing Co., Dordrecht, Holland).
PERSSON, S. E., FROGEL, J. A., AARONSON, M. : *Astrophys. J.* **208,** 753.
PHILLIPS, T. G., KNAPP, G. R., HUGGINS, P. J., WERNER, M. W., WANNIER, P. G., NEUGEBAUER, G., ENNIS, D. : 1981, *Astrophys. J.* **245,** 512.
POTTASCH, S. R. : 1956, *Bull. Astron. Inst. Neth.* **13,** 77.
REIFURTH, B. : 1983, *Astron. Astrophys.* **117,** 183.
ROBINSON, B. J., MCCUTCHEON, W. H., MANCHESTER, R. N., WHITEOAK, J. B. : 1983, *Surveys of the Southern Galaxy,* eds. Burton and Israel (D. Reidel Publishing Co., Dordrecht, Holland).
RODRIGUEZ, L. F., CANTO, J., MORAN, J. M. : 1982, *Astrophys. J.* **255,** 103.
RODRIGUEZ, L. F., MORAN, J. M., DICKINSON, D. F., GYULBUDAGHIAN, A. L. : 1978, *Astrophys. J.* **226,** 115.
SULLIVAN, W. T. : 1973, *Astrophys. J. Suppl.* **25,** 393.
TAPIA, M. : 1981, *Mon. Not. R. Astron. Soc.* **197,** 949.
TURNER, B. E., THADDEUS, P. : 1977, *Astrophys. J.* **211,** 755.
WEAVER, H., DIETER, N. H., WILLIAMS, D. R. W. : 1968, *Astrophys. J. Suppl.* **16,** 219.
WHITE, R. E. : 1977, *Astrophys. J.* **211,** 744.
WILSON, T. L., MEZGER, P. G., GARDNER, F. F., MILNE, D. K. : 1970, *Astron. Astrophys.* **6,** 364.
WOOTTEN, A., SARGENT, A., KNAPP, G., HUGGINS, P. J. : 1983, *Astrophys. J.* **269,** 147.
ZUCKERMAN, B., PALMER, P. : 1974, *A. Rev. Astron. Astrophys.* **12,** 279.

© European Southern Observatory • Provided by the NASA Astrophysics Data System

1986A&AS...65..465P

TABLE I. — *Derived and observed properties for NGC 6334.*

POSITION	T_A^*(CO) J=2-1	T_A^{*+}(CO) J=1-0	T_A^{*+}(^{13}CO) J=1-0	ΔV(2-1) km.sec^{-1}	n(H_2) cm^{-3}	X(CO)/dv/dz km^{-1}sec.pc.	dv/dz km.sec^{-1}.pc^{-1}	Z pc	Z arcmins	M/$M_\odot$	A_v mags
A	27	36	15.7	11.3	$6.0.10^4$	$1.4.10^{-5}$	7.3	1.1	2.1	$1.8.10^3$	$2.8.10^2$
W10 S03	27	31	7.2	8.3	$1.8.10^3$	$8.0.10^{-5}$	1.3	5.8	11.5	$9.1.10^3$	32.2
B	30	32	11.1	5.7	$7.5.10^3$	$3.9.10^{-5}$	2.6	1.5	3.0	$6.7.10^2$	34.9
W20 S06	12	12	3.0	6.1	$1.9.10^3$	$7.8.10^{-5}$	1.3	4.2	8.2	$3.5.10^3$	24.3
C	22	35	8.5	7.4	$3.2.10^3$	$6.0.10^{-5}$	1.7	3.7	7.3	$4.1.10^3$	36.2
W35 509	28	34	6.9	6.7	$1.5.10^3$	$9.4.10^{-5}$	1.2	4.7	9.3	$4.1.10^3$	21.8
W40 510	24	30	5.6	5.7	$1.6.10^3$	$8.5.10^{-5}$	1.2	3.9	7.8	$2.4.10^3$	19.1
D	14	29	7.9	9.6	$3.5.10^3$	$5.7.10^{-5}$	1.8	3.3	6.5	$3.3.10^3$	35.6

+ *Adapted from Dickel et al. (1977).*

© European Southern Observatory • Provided by the NASA Astrophysics Data System

1986A&AS...65..465P

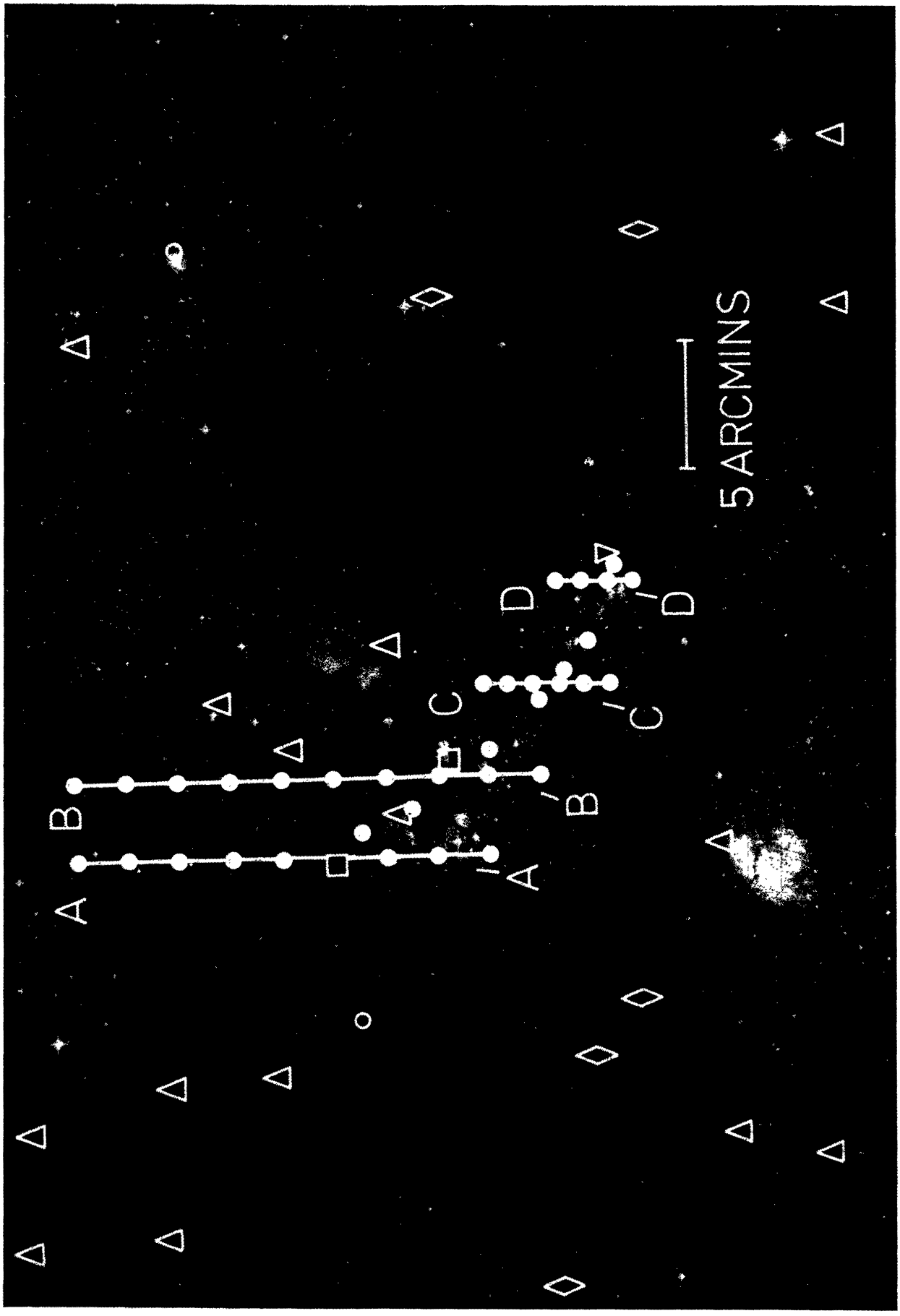

FIGURE 1. — SERC Southern survey J plate of the NGC 6334 complex. The CO beam locations are noted by filled circles, with the four traverses (east to west) respectively intersecting sources A through D. The various symbols indicate IRAS source positions, and correspond to the following flux ranges : Δ — NIR detections ($\lambda < 25$ μm); $\diamond - F_\nu$ ($\lambda = 60$ μm) $< 10^2$ Jy ; $0 - 10^2$ Jy $< F_\nu$ ($\lambda = 60$ μm) $< 10^3$ Jy ; $\square - 10^3$ Jy $< F_\nu$ ($\lambda = 60$ μm) $< 10^4$ Jy ; $\nabla - F_\nu$ ($\lambda = 60$ μm) $> 10^4$ Jy. In certain cases only longer wave ($\lambda \simeq 100$ μm) fluxes are available, and the categorisation based on 60 μm measures is therefore approximate.

© European Southern Observatory • Provided by the NASA Astrophysics Data System

1986A&AS...65..465P

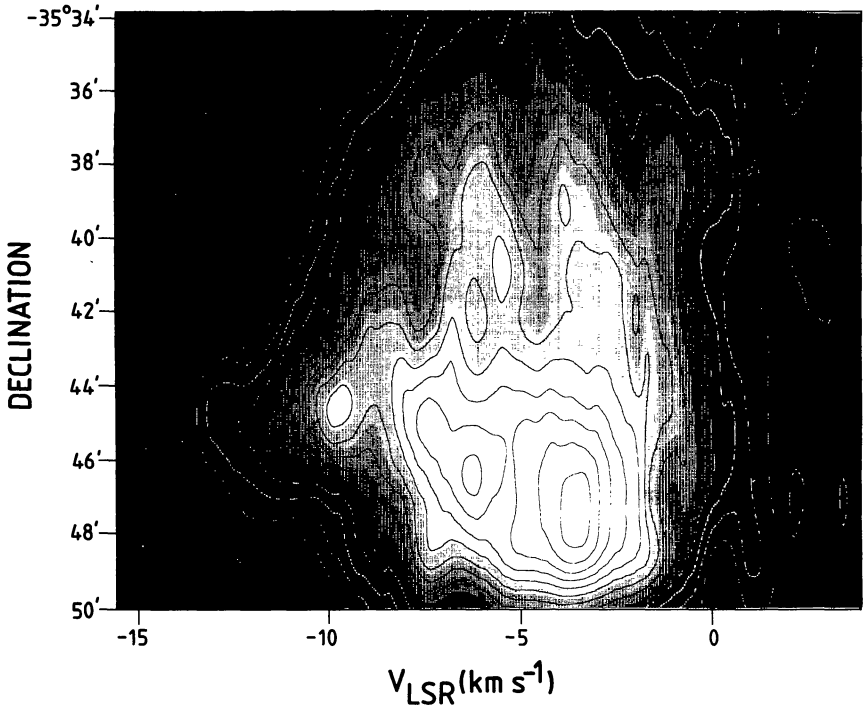

FIGURE 2. — CO $J = 2 - 1$ spatial-velocity map for NGC 6334(A). The lowest contour levels correspond to $T_A^* = 2$ K, with subsequent contours incrementing in units of 2 K.

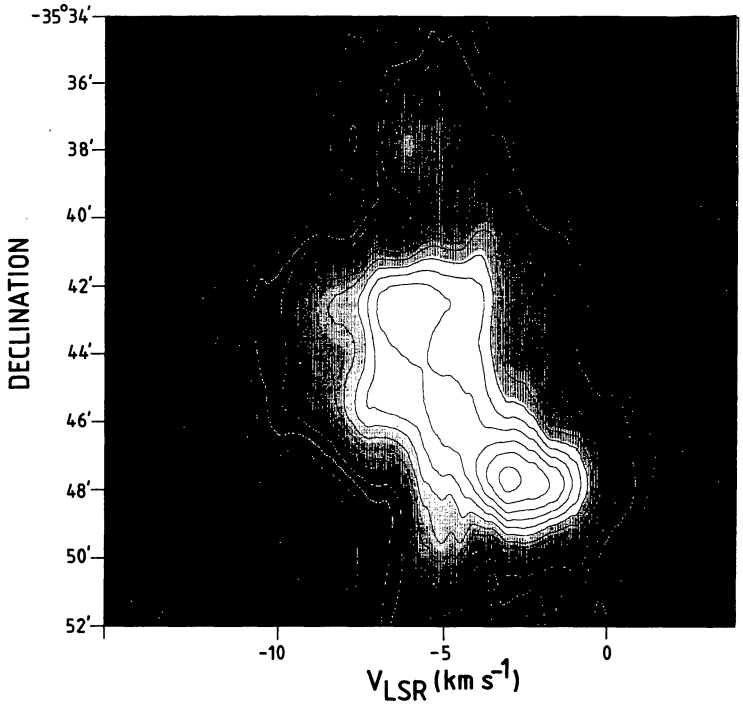

FIGURE 3. — CO $J = 2 - 1$ spatial-velocity map for NGC 6334 (B). Contour levels are the same as for figure 2.

© European Southern Observatory • Provided by the NASA Astrophysics Data System

1986A&AS...65..465P

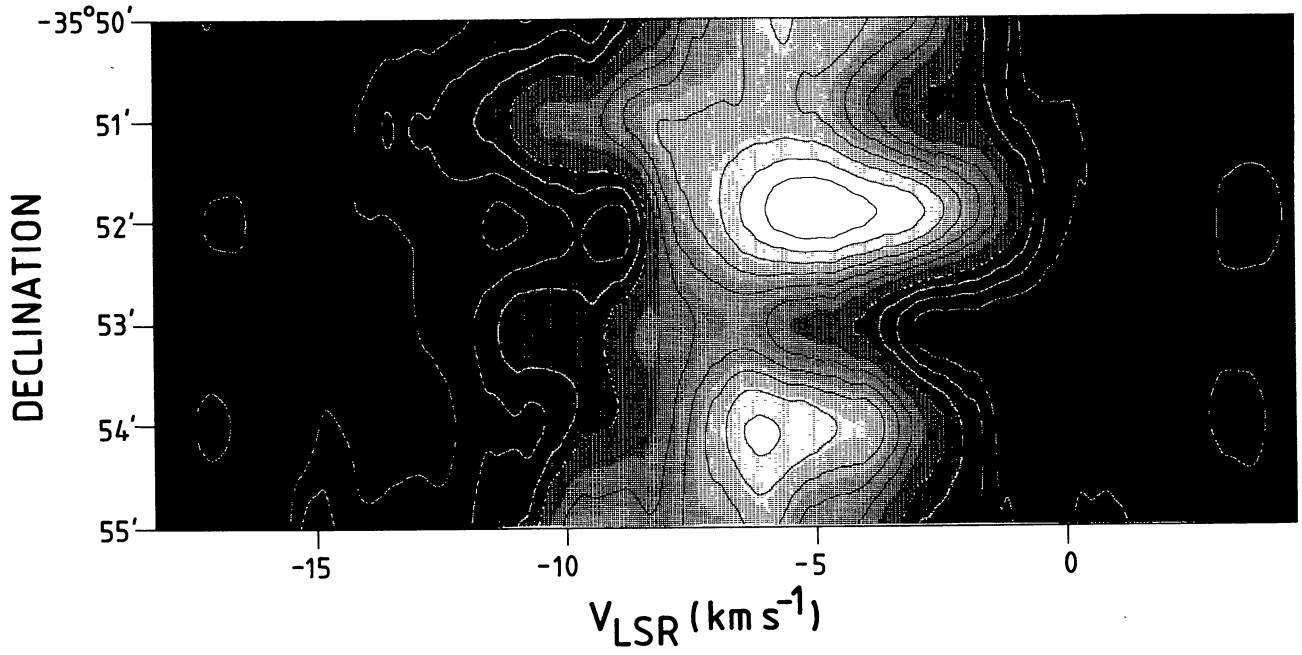

FIGURE 4. — CO $J = 2 - 1$ spatial-velocity map for NGC 6334 (C). Contour levels are as specified in figure 2.

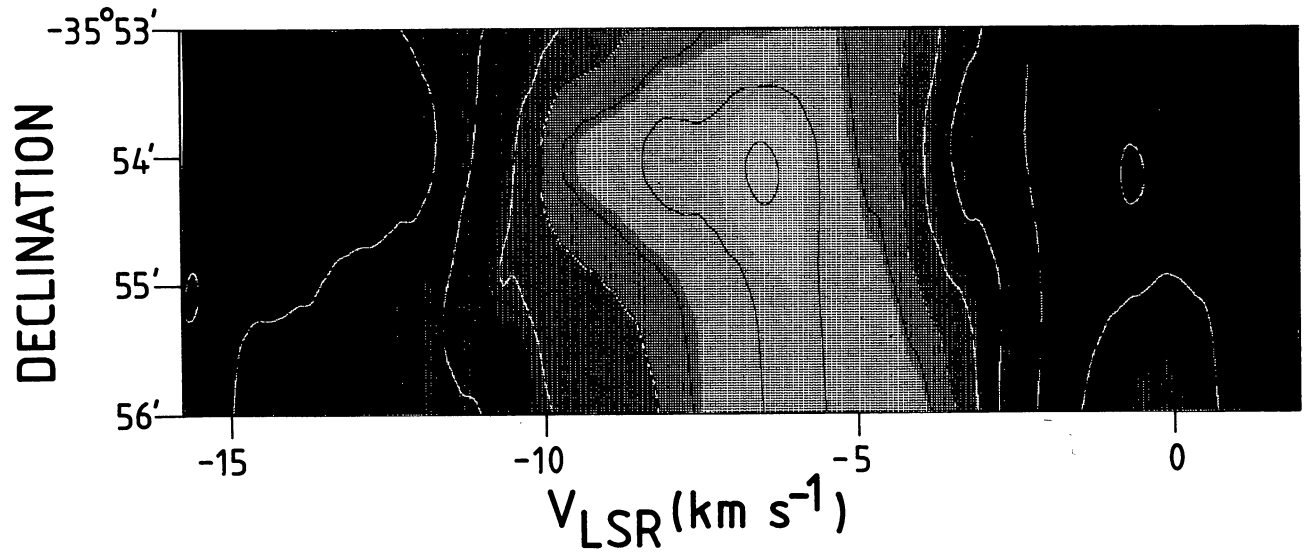

FIGURE 5. — CO $J = 2 - 1$ spatial-velocity map for NGC 6334 (D). Contour levels are as specified in figure 2.

© European Southern Observatory • Provided by the NASA Astrophysics Data System

1986A&AS...65..465P

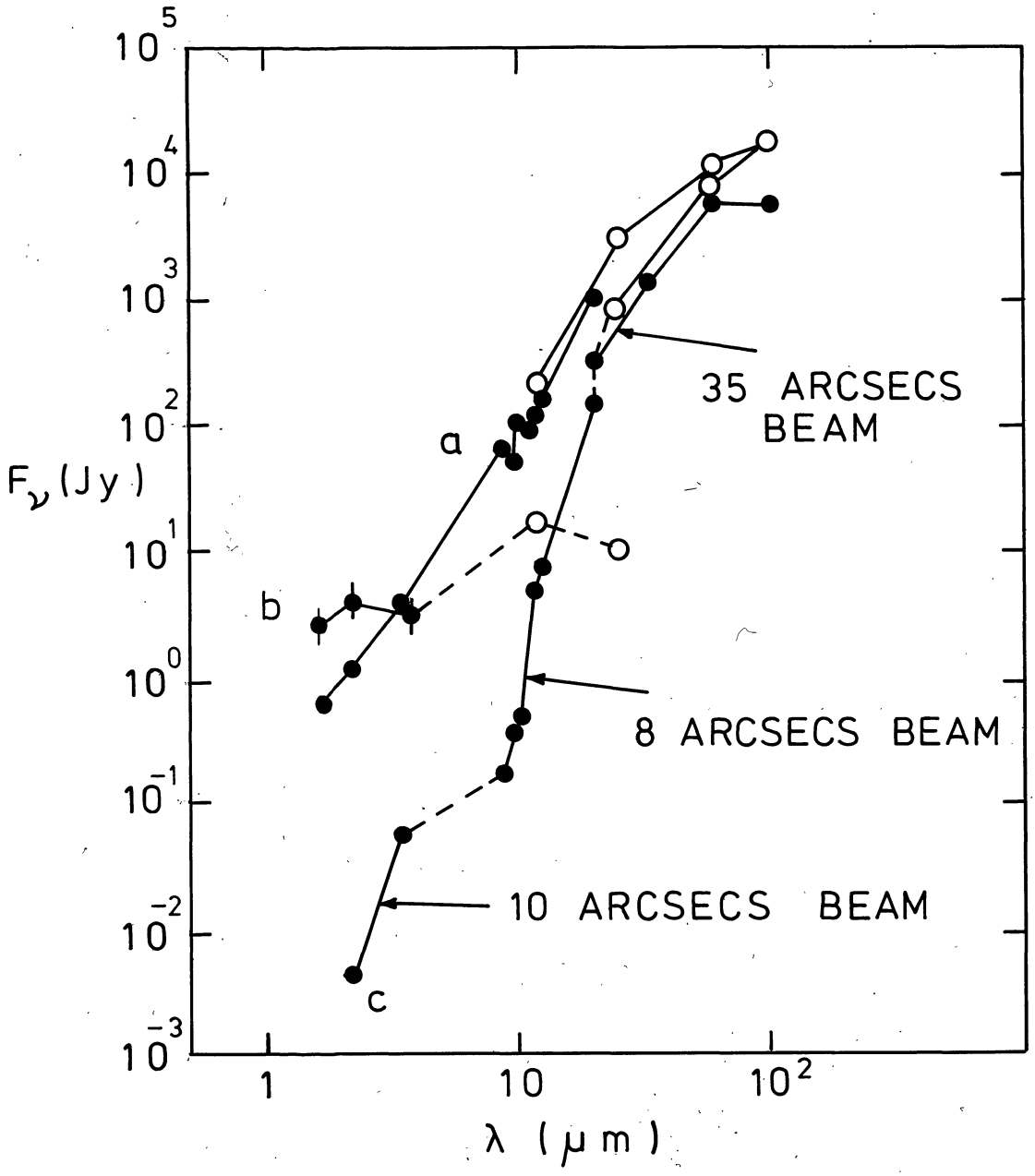

FIGURE 6. — Spectra for selected sources in or near NGC 6334, IC 4628, and NGC 6193. For all cases, open circles correspond to IRAS flux densities. a) RCW 108 - shorter wave data is from Frogel and Persson (1974) and Persson *et al.* (1976) ; b) IC 4628 (Source A) - shorter wave data are from Danks (1975) ; c) NGC 6334 (D) - the shorter wave data is from Harvey and Gatley (1983), where the NIR results refer to IRS 3.

© European Southern Observatory • Provided by the NASA Astrophysics Data System

1986A&AS...65..465P

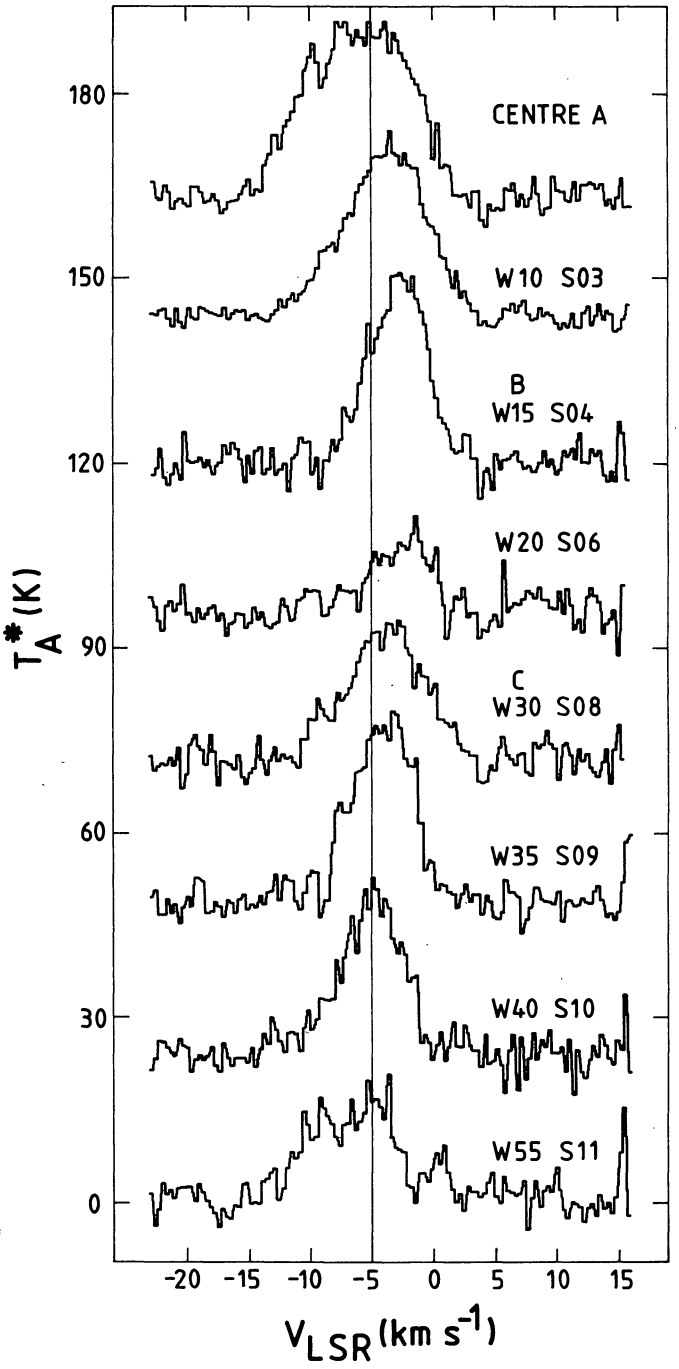

FIGURE 7a. — Selected CO $J = 2 - 1$ spectra for various locations in the NGC 6334 complex ; positions are with respect to source A (α (1950) = 17 h 17 min 32 s ; δ (1950) = $-$ 35° 44′).

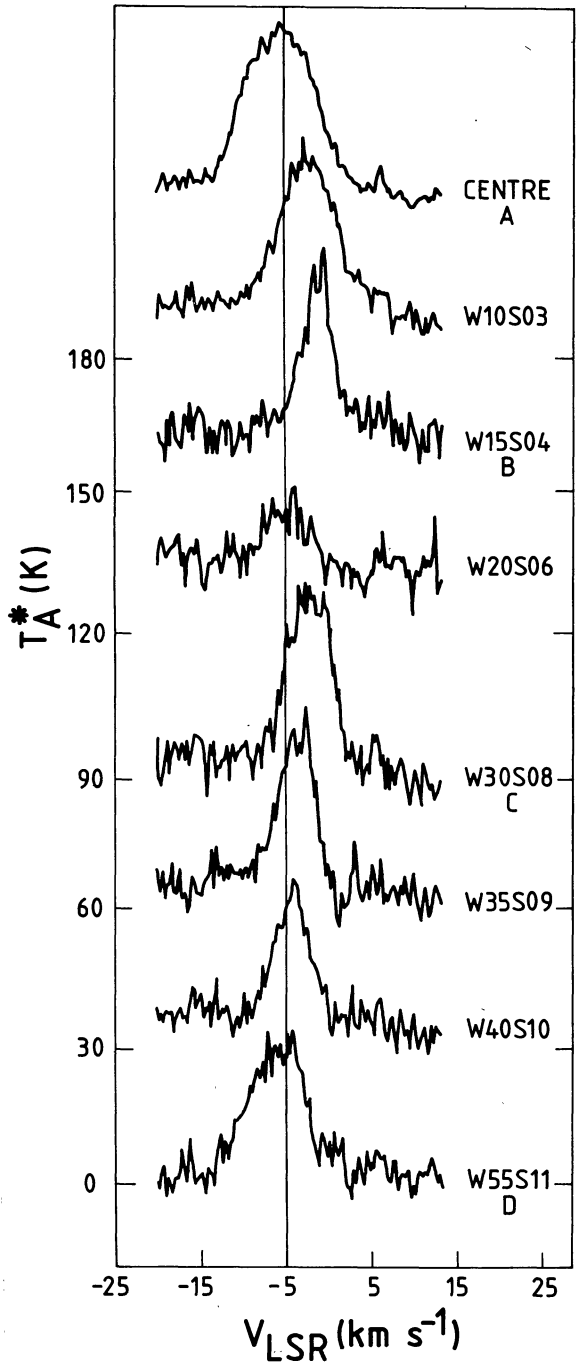

FIGURE 7b. — CO $J = 1 - 0$ spectra from Dickel *et al.* (1977) for the same locations as in figure 7a. Note that the velocity and temperature scales differ from figure 7a.

© European Southern Observatory • Provided by the NASA Astrophysics Data System

1986A&AS...65..465P

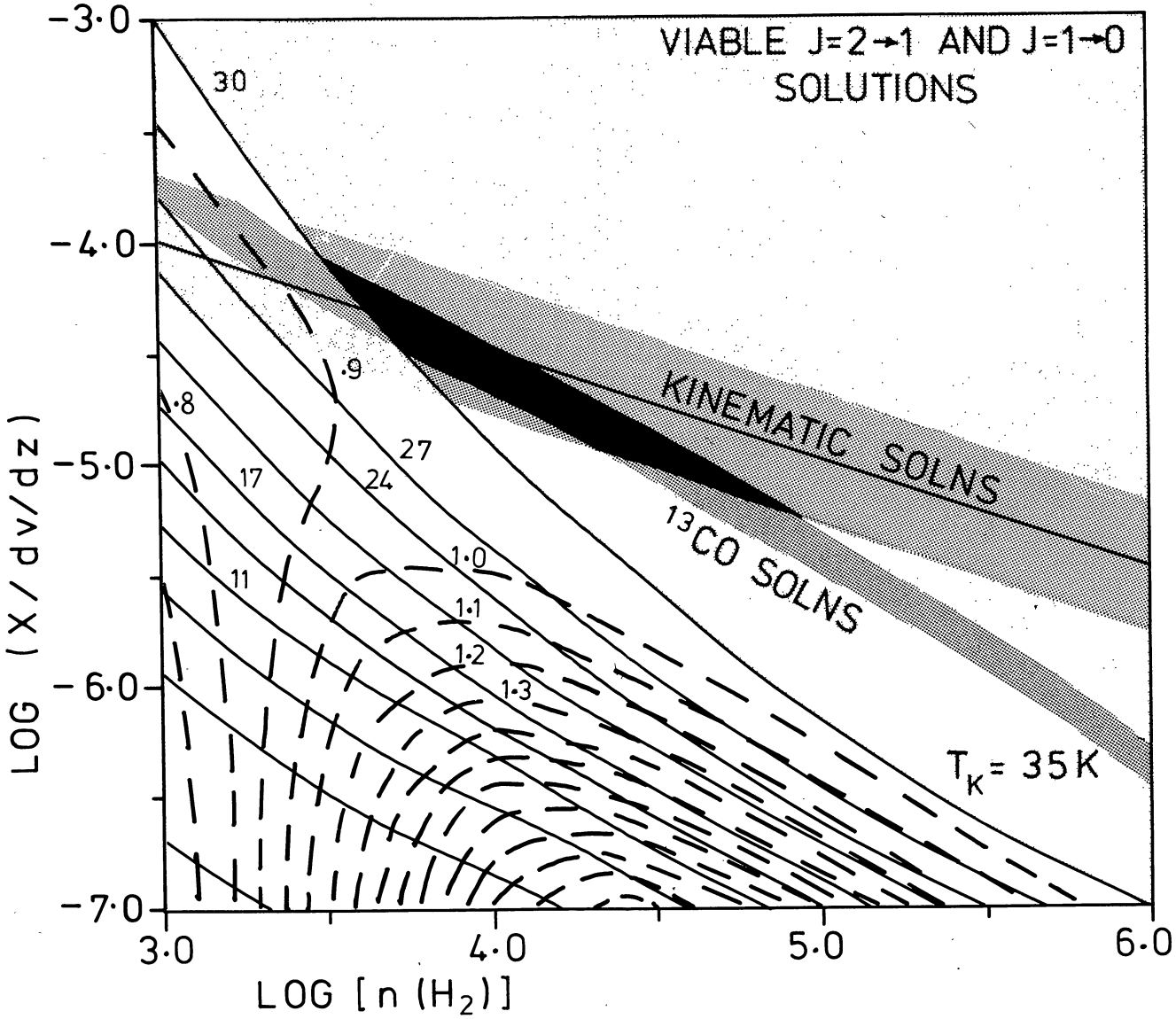

FIGURE 8. — Representative LVG analysis for mean spectra based on figures 7a and 7b, and the corresponding ^{13}CO ($J = 1 - 0$) data of Dickel *et al.* (1977). The kinetic temperature is taken as $T_k = 35$ K, and $X(CO)/dv/dz$ is in units of km^{-1} . s. pc. Solid curves correspond to the $J = 1 - 0$ antenna temperature, and dashed lines refer to the ratio $T_A^*(J = 2 - 1)/T_A^*(J = 1 - 0)$. The broad shaded region to the right of the $T_A^*(J = 1 - 0) = 30$ K curve corresponds to the region where viable $J = 1 - 0$ and $J = 2 - 1$ solutions occur. The diagonal ^{13}CO band indicates the error bound within which ^{13}CO $J = 1 - 0$ solutions are permissible. Finally, the kinematic solutions refer to the regime where $X(CO)/dv/dz \simeq 3.38 \times 10^{-3}\langle n(H_2)\rangle^{-1/2}$ (see text). The intersection of the curves is used to define specific values for $n(H_2)$, and $X(CO)/dv/dz$.

© European Southern Observatory • Provided by the NASA Astrophysics Data System

1986A&AS...65..465P

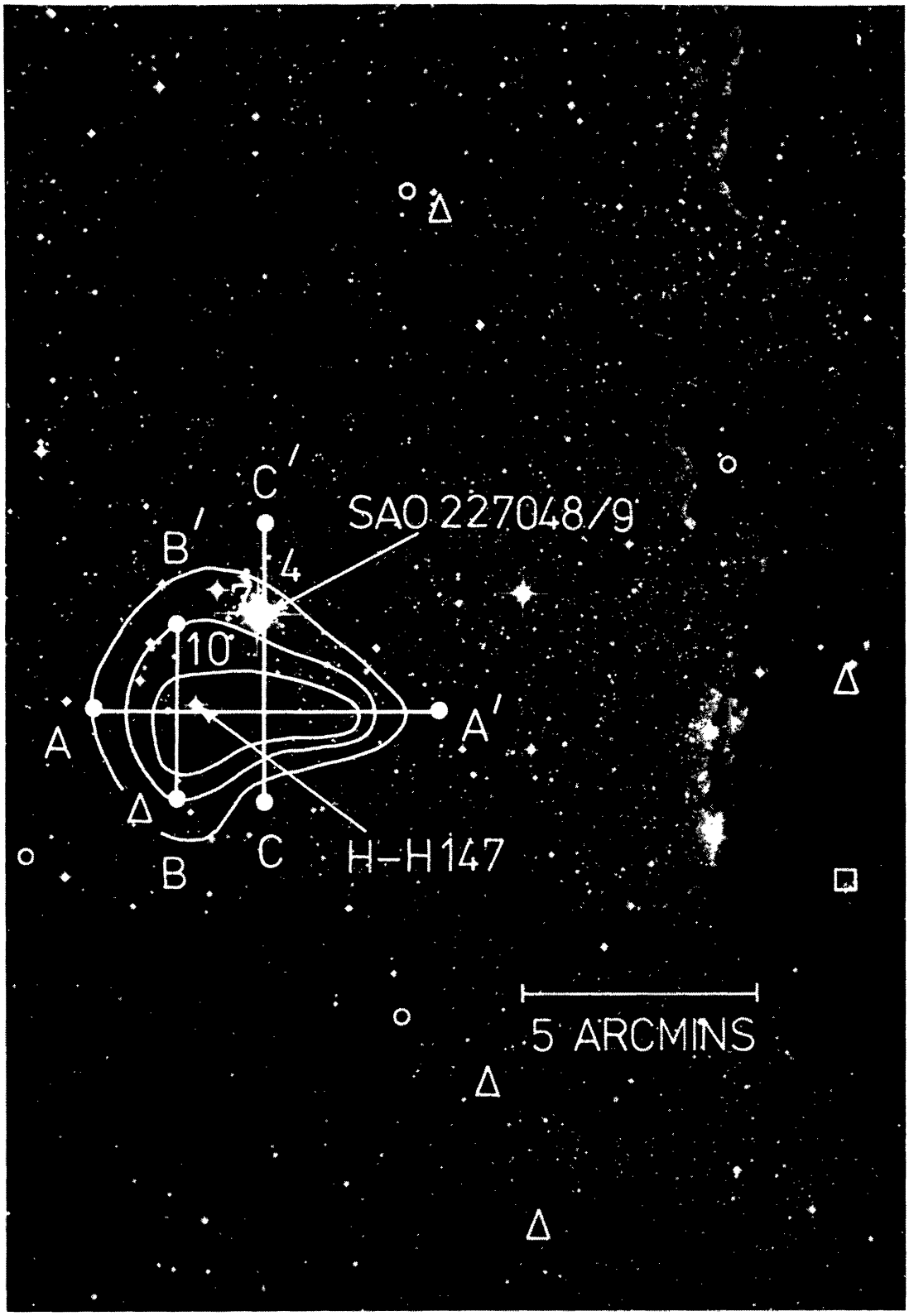

FIGURE 9. — SERC Southern Survey SR plate of the cluster NGC 6193. The contours (in units of peak T_A^*) delineate the CO $J = 2 - 1$ cloud, whilst individual symbols again refer to IRAS source positions, and correspond to the following flux ranges: Δ — NIR Detection ($\lambda < 25\ \mu m$); 0 — F_ν ($60\ \mu m$) $< 10^3$ Jy; $\square$ — F_ν ($60\ \mu m$) $> 10^3$ Jy. SAO 27048/9 are the central ~ 05 stars for this cluster, whilst H-H 147 is a bright G5 star noted by Herbst and Havlen (1977) and discussed in section 3.

© European Southern Observatory • Provided by the NASA Astrophysics Data System

1986A&AS...65..465P

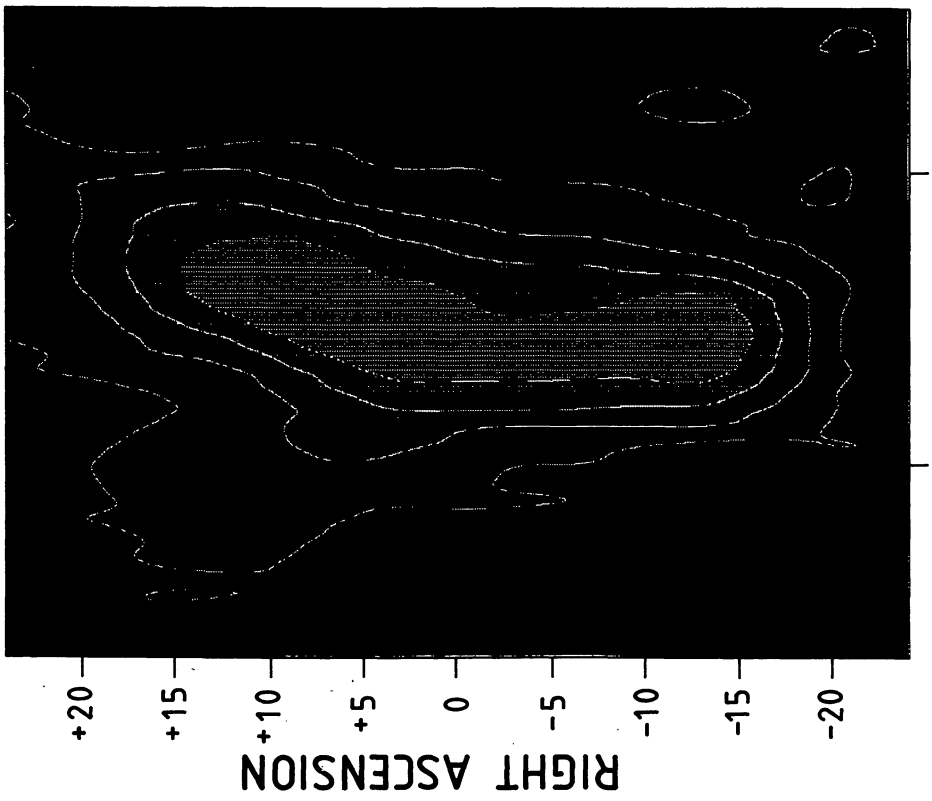

FIGURE 11. — Spatial-velocity axis A-A′ in figure 9, with RA offsets in seconds of time. Contour levels are as in figure 10, and east is to the top. The declination of this map is δ (1950) = − 48° 42′, and the right ascension offset zero is α (1950) = 16 h 37 min 35 s.

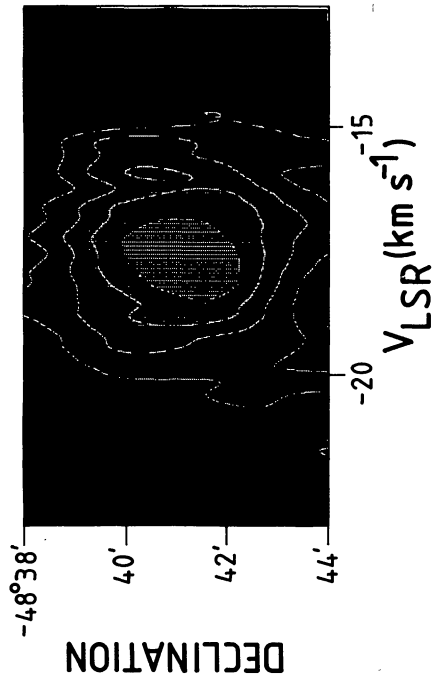

FIGURE 10. — Spatial-velocity map for the axis C-C′ in figure 9 (α (1950) = 16 h 37 min 35 s). The lowest level corresponds to T_A^* = 2.5 K, with subsequent contours corresponding to increments of 2.5 K.

© European Southern Observatory • Provided by the NASA Astrophysics Data System

1986A&AS...65..465P

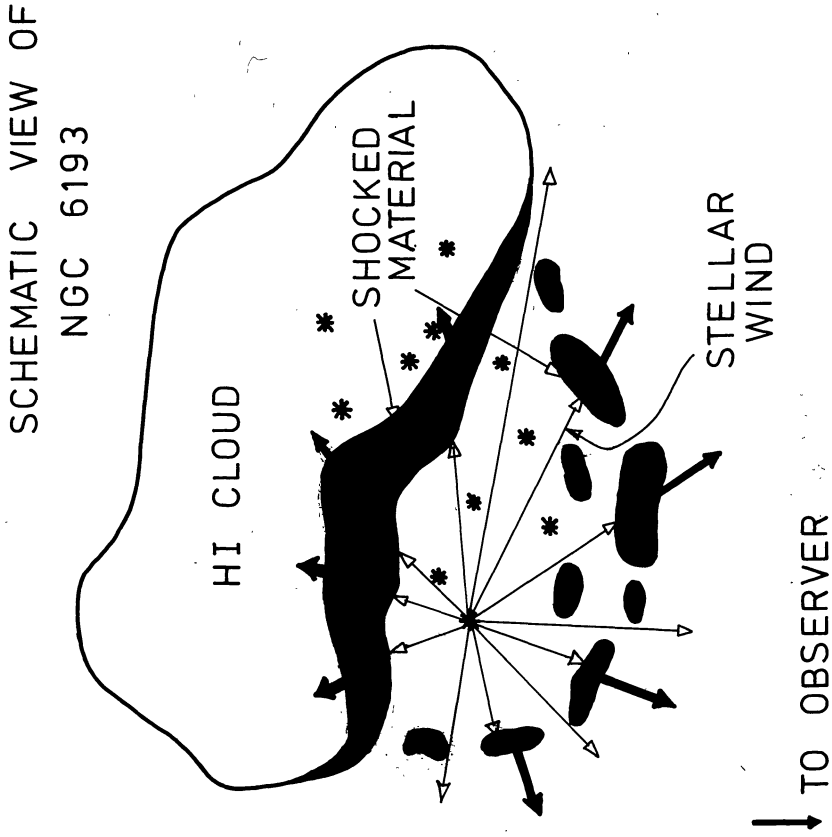

FIGURE 13. — Schematic diagram of NGC 6193, where east is to the left, and west to the right. For this model, a stellar wind leads to shock compression and dispersion of ambient cluster material. Low-mass fragments are accelerated towards the observer at a relative velocity $V \sim +5$ km . s^{-1}, whilst a more massive post-shock zone travels into the HI cloud at velocity $V \sim +1$ km . s^{-1}.

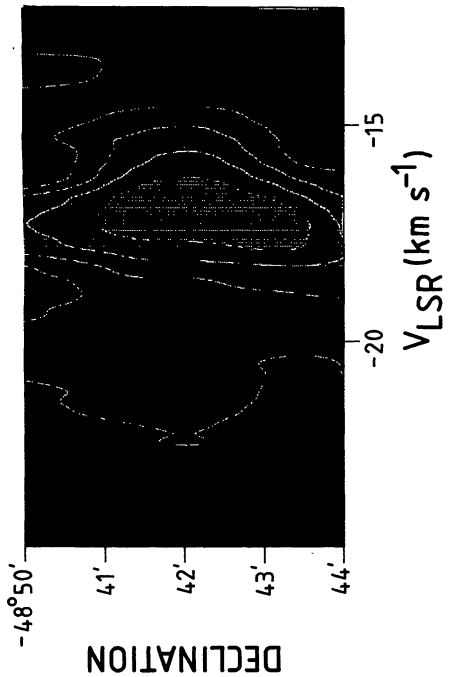

FIGURE 12. — Spatial-velocity map for axis B-B' (α (1950) = 16 h 37 min 47 s). Contour values are the same as in figure 10.

© European Southern Observatory • Provided by the NASA Astrophysics Data System

1986A&AS...65..465P

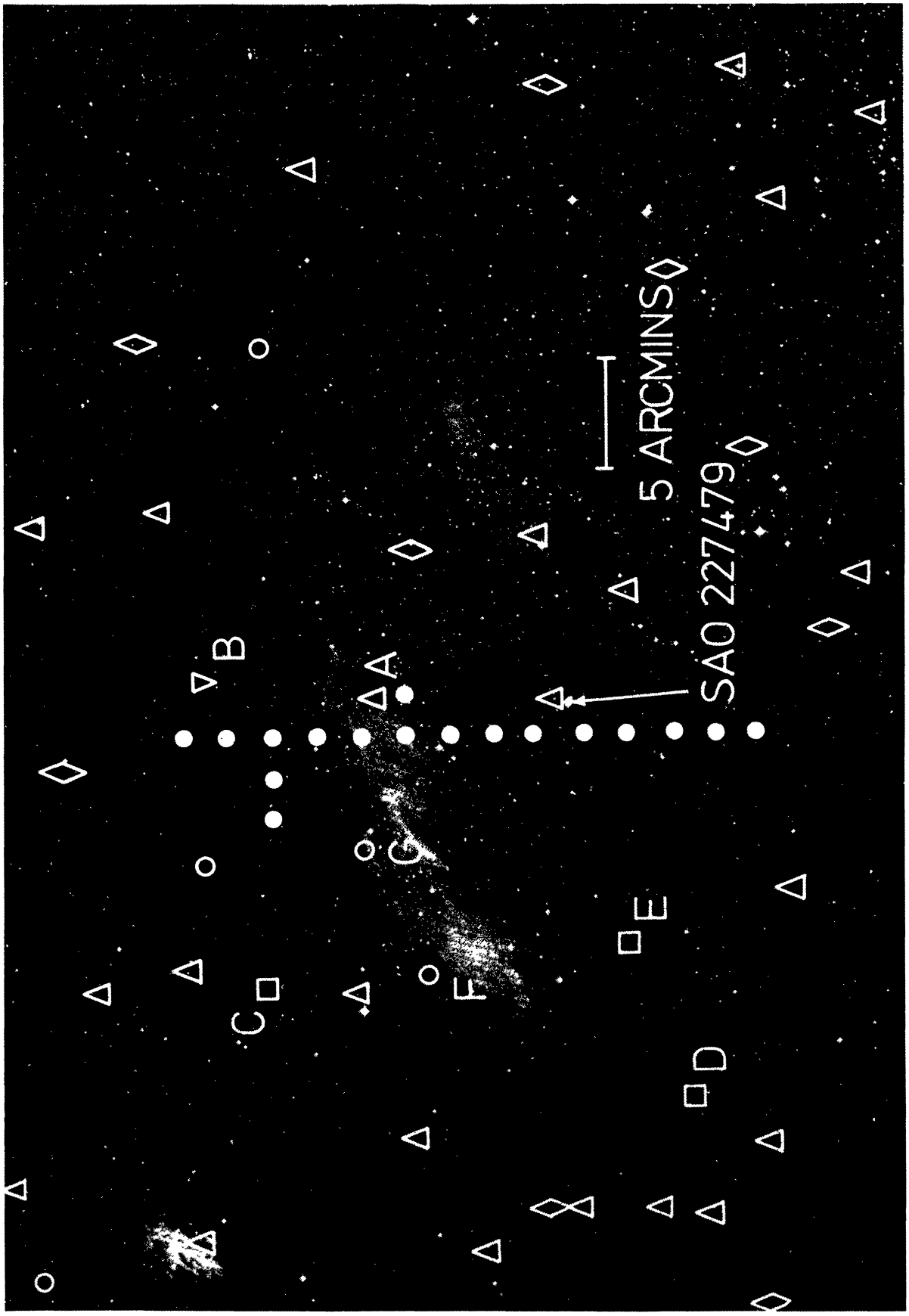

FIGURE 14. — An SERC Southern Survey SR plate of the nebula IC 4628. The filled circles correspond to CO $J = 2 - 1$ beam locations. Other symbols correspond to IRAS source positions ; Δ — NIR ($\lambda < 25$ μm) detections ; $\diamond$ — F_ν ($\lambda = 100$ μm) $< 10^2$ Jy ; 0 — 10^2 Jy $< F_\nu$ (100 μm) $< 10^3$ Jy ; □ — 10^3 Jy $< F_\nu$ (100 μm) $< 10^4$ Jy ; ∇ — F_ν (100 μm) $> 10^4$ Jy. Source A appears coincident (within errors) to the NIR source found by Danks (1975). Finally SAO 227479 (HD 152723) represents the central (and most luminous visual) star for the cluster Tr 24.

© European Southern Observatory • Provided by the NASA Astrophysics Data System

1986A&AS...65..465P

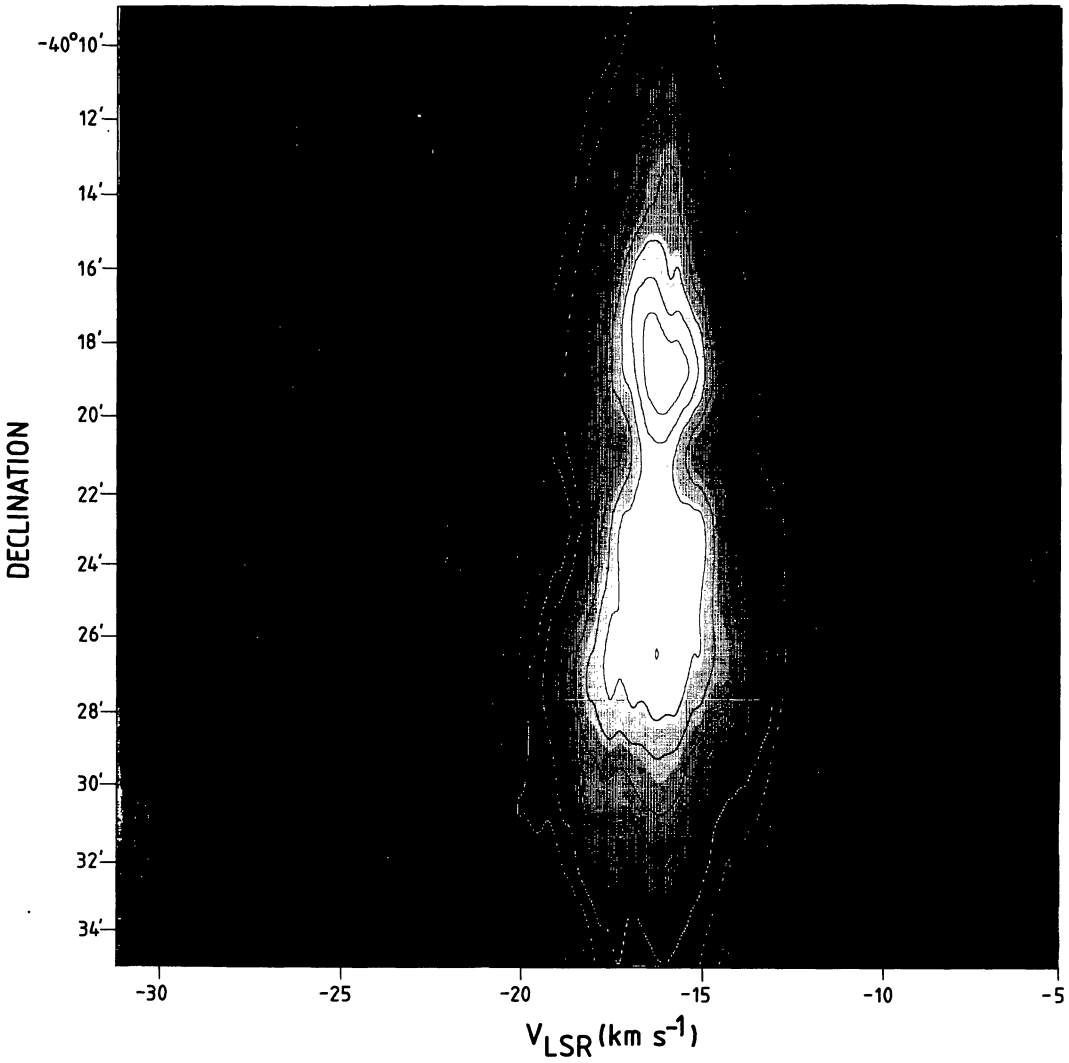

FIGURE 15. — Spatial-velocity map for the traverse in figure 14 (α (1950) = 16 h 53 min 33 s). The lowest contour corresponds to $T_A^* = 2.5$ K, and higher contours represent further increments of 2.5 K.

© European Southern Observatory • Provided by the NASA Astrophysics Data System

1986A&AS...65..465P

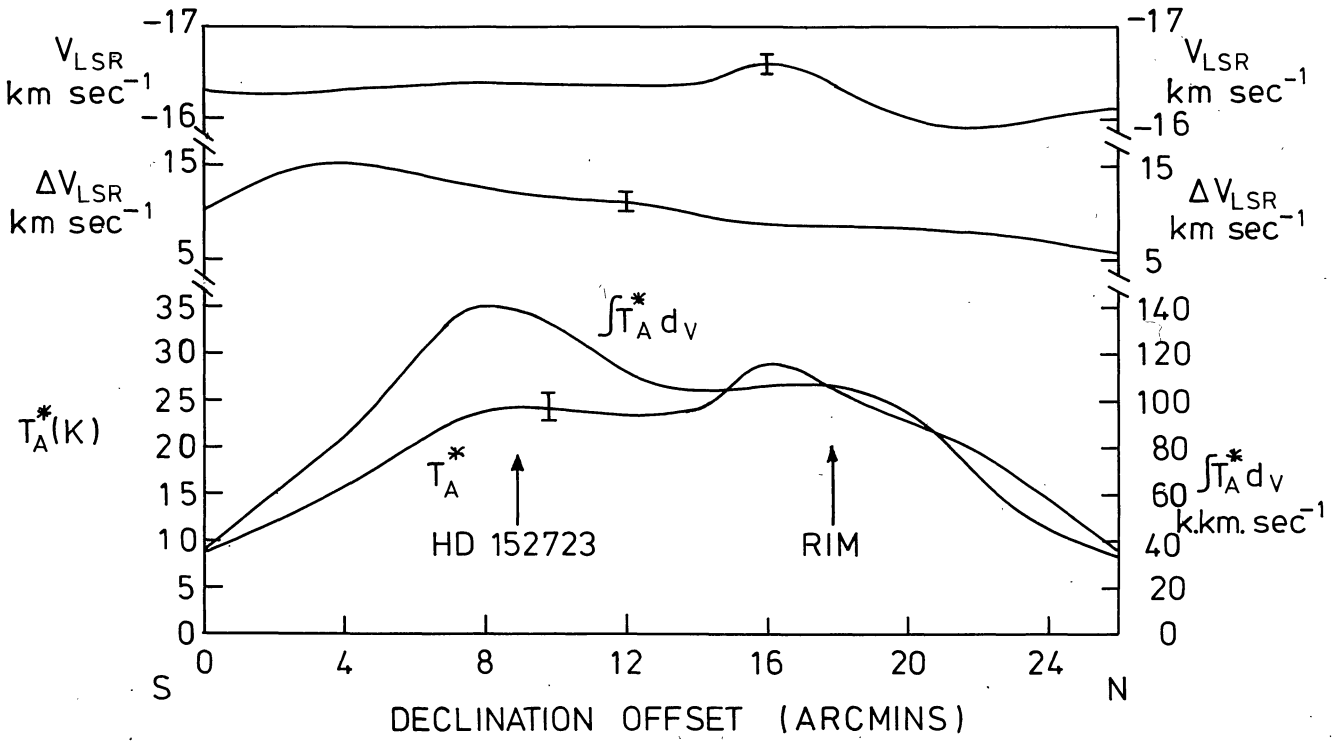

FIGURE 16. — Variation of IC 4628 CO $J = 2 - 1$ central line velocity V_{lsr}, line FWHM ΔV, peak antenna temperature T_A^*, and velocity integral $\int T_A^* \, dv$ as a function of declination (where offset zero corresponds to $\delta = -40° 35'$). HD 152723 is the central O star for the cluster Tr 24.

© European Southern Observatory • Provided by the NASA Astrophysics Data System

1986A&AS...65..465P

ASTRONOMY & ASTROPHYSICS
SUPPLEMENT SERIES

SEPTEMBER 1986, PAGE 485

Astron. Astrophys. Suppl. Ser. **65**, 485-496 (1986)

Spectral flux densities of radio sources at 22 MHz

R. S. Roger, C. H. Costain and D. I. Stewart

Dominion Radio Astrophysical Observatory, Herzberg Institute of Astrophysics, Box 248, Penticton, B.C. Canada V2A 6K3

Received November 29, accepted December 24, 1985

Summary. — We present a compilation of the flux densities at 22.25 MHz for 395 radio sources. The flux densities are derived from three or more observations of each source. The sources were measured over a period of several years with the T-shaped radiotelescope at the Dominion Radio Astrophysical Observatory.

Key words : radio sources : general — radio continuum — galaxies : radio.

1. Introduction.

The 22 MHz T-shaped radiotelescope at the Dominion Radio Astrophysical Observatory (Costain *et al.*, 1969) was used for several years both to survey galactic background emission and for observations of discrete (mostly unresolved) radio sources stronger than the confusion limit of ~ 30 Jy. The flux densities for 220 sources measured with the telescope have been reported (Roger *et al.*, 1969 (Paper I) ; Roger *et al.*, 1973). In this paper we present a final list of the flux densities scaled both from the specific observations of individual sources and from scans of the survey of galactic emission. The list comprises revised flux densities of sources listed in paper I and new flux densities for sources measured subsequently.

2. The 22 MHz telescope.

The telescope consists of an array of 624 dipoles arranged in the form of a « T » above a reflecting screen of area 65000 m^2. An instantaneous beam of size 66′ (EW) by 102′ (NS) at the zenith was produced by phase-switching the east-west arm with the north arm and detecting the correlated component. The signal from the dipoles in the overlap area common to both arms was split and fed separately to both parts, thus ensuring that the correlated output contained all spatial components down to the resolution of the telescope. The array could be phased to move the beam off the zenith in the meridian plane with consequent north-south broadening of the beam proportional to the secant of the zenith angle. In the « survey » mode-of-operation the telescope beam was cycled through phasings for five adjacent declinations in a time short compared to the sample time in the hour-angle dimension. Since there was no provision for phasing the array in the east-west direction, all observations were made at meridian transit. Further details of the telescope are described by Costain *et al.* (1969).

Send offprint requests to : R. S. Roger.

3. The observing conditions.

Observations of point sources at 22 MHz can be severely affected by conditions in the Earth's ionosphere. Small-scale irregularities in electron density cause the signal to scintillate on a time scale of 10 to 100 s. Large-scale gradients in density, with both regular and irregular components, produce refraction which at times can amount to 20′. Since ionospheric conditions are not readily predictable, it is often necessary to observe each source on ten or more occasions in order to obtain sufficient measurements free of propagation defects to provide a reliable estimate of flux density.

Owing to ionospherically propagated man-made interference, regular observations during daytime hours were possible only during the years near sunspot minimum, when critical frequencies in the F-region are too low to sustain such propagation. These daytime observations required a correction for D-region absorption, typically amounting to 15 % near midday. This correction was derived from 22 MHz riometer measurements made on site (see Paper I). Nighttime absorption was generally less than 4 % and was not corrected for.

4. The flux densities.

Because of the « total-power » nature of the detected output, most radio sources ($S \leq 200$ Jy) appear as small deflections on top of the non-thermal galactic background emission. Relatively isolated sources were scaled « by computer » with a cubic fit to the background emission before and after transit (Paper I). However, because of the proximity of nearby sources and structure in the background emission, the majority of sources were « hand-scaled » from the right-ascension scans.

© European Southern Observatory • Provided by the NASA Astrophysics Data System

1986A&AS...65..465P

All flux densities are measured with respect to a reference flux density for Cygnus A (3C405) of 29100 Jy at 22 MHz. A complete description of this scale and comparisons with other low-frequency scales are given in Roger *et al.* (1973). That paper reported substantial agreement between this (Penticton) scale and the Clark Lake 26.3 MHz scale (Viner and Erickson, 1975). A discrepancy between these two scales and the 20-25 MHz Grakovo UTR-1 scale (Braude *et al.*, 1970) has been largely resolved with the newly calibrated Grakovo UTR-2 scale (Braude, 1978).

The continuity of the calibration was ensured by the injection of a controlled level of correlated noise in alternate integration samples.

Table I contains the compilation of the flux densities. The sources are ordered in right ascension with a designation (Column 1) representing the 1950 coordinates. Column 2 contains other catalogue designations. The flux densities and their errors are listed in columns 3 and 4. Column 5 indicates the number of separate observations with contribute to the final flux density. A nearby source listed in column 6 may affect the accuracy of the measurement. Doubtful identification of a confusing source is indicated by parentheses. A nearby source which is not listed in higher frequency catalogues is shown as a « not previously catalogued source (NPCS) » together with its 1950 right ascension. A cross (X) in column 7 indicates that the complexity of the galactic background emission in the neighbourhood of the source may have affected the measurement. Specific sources or their sidelobes (sl) which may contribute to the background complexity are listed in column 7. Notes on individual sources are indicated in column 8 and follow the table. The notes include cross references to other low-frequency measurements made with the Clark Lake 26 MHz radiotelescope (Viner and Erickson, 1975) and the Grakovo UTR-2 telescope (Braude *et al.*, 1978, 1979, 1980, 1985).

The Dominion Radio Astrophysical Observatory is operated as a national facility by the National Research Council of Canada.

References

BRAUDE, S. Ya. : 1977, *IAU Symp.* **74,** eds. D. L. Jauncey (Reidel, Dordrecht), p. 9.
BRAUDE, S. Ya., MEGN, A. V., RASHKOVSKI, S. L., RYABOV, B. P., SHARYKIN, N. K., SOKOLOV, K. P., TKATCHENKO, A. P., ZHOUCK, I. N. : 1978, *Astrophys. Space Sci.* **54,** 37.
BRAUDE, S. Ya., MEGN, A. V., RYABOV, B. P., ZHOUCK, I. N. : 1970, *Astrophys. Space Sci.* **8,** 275.
BRAUDE, S. Ya., MEGN, A. V., SOKOLOV, K. P., TKACHENKO, A. P., SHARYKIN, N. K. : 1979, *Astrophys. Space Sci.* **64,** 73.
BRAUDE, S. Ya., MIROSHNITCHENKO, A. P., SOKOLOV, K. P., SHARYKIN, N. K. : 1981, *Astrophys. Space Sci.* **74,** 409.
BRAUDE, S. Ya., SHARYKIN, N. K., SOKOLOV, K. P., ZAKCHARENKO, S. M. : 1985, *Astrophys. Space Sci.* **111,** 237.
COSTAIN, C. H., LACEY, J. D., ROGER, R. S. : 1969, IEEE Trans. Antennas Propag. AP-17, 162.
ROGER, R. S., BRIDLE, A. H., COSTAIN, C. H. : 1973, *Astron. J.* **78,** 1030.
ROGER, R. S., COSTAIN, C. H., LACEY, J. D. : 1969, *Astron. J.* **74,** 366.
VINER, M. R., ERICKSON, W. C. : 1975, *Astron. J.* **80,** 931.

TABLE I : *notes*

C. A 26.3 MHz flux density measured at Clark Lake is given by Viner and Erickson (1975)
G1, G2, G3, G4. Low frequency flux densities measured at Grakovo are given by Braude *et al.* (1978), (1979), (1981), (1985) respectively.

1. See notes for this source in Roger *et al.* (1973).
2. Comprises 3C66A and 3C66B and possibly a broad emission component.
3. Confusing sources surrounding 3C196 or emission from broad region centered on the source : near Abell 637.
4. Transits 0.8 min earlier than 4C14.31, near right ascension of Abell 795.
5. Evidence of E-W broadening.
6. Confused region ; other sources not catalogued. Alternative interpretation with source on broad background feature gives a flux density of 128 ± 20.
7. Broad emission centred on 3C298 ($\sim 50'$ EW).
8. Extended source, corrected for broadening.
9. Right ascension 45^s later than listed in 4C (lobe shift ?).
10. Possibly extended.
11. Primary calibration source.
12. Confused region.
13. Epoch 1966.5.

© European Southern Observatory • Provided by the NASA Astrophysics Data System